The Asynchronous State in Cortical Circuits
Alfonso Renart, *et al.*
Science **327**, 587 (2010);
DOI: 10.1126/science.1179850

small stimuli, barely covering the neurons' receptive fields, are used.
29. A. Renart *et al.*, *Science* **327**, 587 (2010).
30. V. Braitenberg, A. Schüz, *Anatomy of the Cortex: Statistics and Geometry* (Springer, Berlin, 1991).
31. B. Hellwig, A. Schüz, A. Aertsen, *Biol. Cybern.* **71**, 1 (1994).
32. J. de la Rocha, B. Doiron, E. Shea-Brown, K. Josić, A. Reyes, *Nature* **448**, 802 (2007).
33. Y. C. Yu, R. S. Bultje, X. Wang, S. H. Shi, *Nature* **458**, 501 (2009).
34. J. Hertz, *Neural Comput.*, published online 20 October 2009; 10.1162/neco.2009.06-08-806.

35. We thank M. Subramanian, A. Hoenselaar, T. J. Williford, and D. Murray for help with experiments; R. J. Cotton for his contribution in setting up recording equipment; and the Siapas laboratory at Caltech for providing the recording software. We thank R. J. Cotton, P. Dayan, S. Deneve, K. D. Harris, E. V. Lubenov, W. J. Ma, J. H. Macke, A. Renart, J. de la Rocha, A. G. Siapas, and S. M. Smirnakis for comments on the manuscript and discussions. This work was supported by the National Eye Institute, NIH (R01 EY018847), the Max Planck Society, the U.S. Department of Defense (W81XWH-08-2-0147), a VA Merit Award from the Department of Veterans Affairs, and an Arnold and Mabel Beckman Foundation Young Investigator Award to A.S.T., and by the German Federal Ministry of Education and Research (BMBF) through the Bernstein award to M.B. (FKZ:01GQ0601).

Supporting Online Material

www.sciencemag.org/cgi/content/full/327/5965/584/DC1
Materials and Methods
SOM Text
Figs. S1 to S9
References

29 July 2009; accepted 10 December 2009
10.1126/science.1179867

The Asynchronous State in Cortical Circuits

Alfonso Renart,[1]*‡ Jaime de la Rocha,[1,2]* Peter Bartho,[1,3] Liad Hollender,[1] Néstor Parga,[4] Alex Reyes,[2] Kenneth D. Harris[1,5]†

Correlated spiking is often observed in cortical circuits, but its functional role is controversial. It is believed that correlations are a consequence of shared inputs between nearby neurons and could severely constrain information decoding. Here we show theoretically that recurrent neural networks can generate an asynchronous state characterized by arbitrarily low mean spiking correlations despite substantial amounts of shared input. In this state, spontaneous fluctuations in the activity of excitatory and inhibitory populations accurately track each other, generating negative correlations in synaptic currents which cancel the effect of shared input. Near-zero mean correlations were seen experimentally in recordings from rodent neocortex in vivo. Our results suggest a reexamination of the sources underlying observed correlations and their functional consequences for information processing.

The spiking activity of neurons is often correlated within local cortical populations (*1*–*4*). Although correlations could be a signature of active information processing (*5*, *6*), they can also impair the estimation of information conveyed by the firing rates of neural populations (*7*, *2*, *8*) and might limit the efficiency of an organism for performing sensory discriminations (*7*, *2*). Under special conditions, correlated spiking is an inevitable consequence of shared presynaptic input (*9*, *10*). In general, however, the overall contribution of shared input to correlation magnitudes measured in vivo is unclear, as measured correlations could reflect mostly covariations in activity due to cognitive or external variables outside the control of the experimenter (*11*–*13*). To investigate the relation between correlations and shared input, we studied theoretically the correlation structures characteristic of densely connected recurrent networks.

We start by considering how the correlation between a single neuronal pair depends on the fraction p of shared inputs and the degree r_{in} to which the inputs are themselves correlated. The effect of shared input can be isolated by considering presynaptic neurons that fire independently ($r_{in} = 0$). Both excitatory (E) and inhibitory (I) shared inputs cause positive correlations of a moderate magnitude in the synaptic input and spiking activity of the postsynaptic pair (Fig. 1, A and B) (*9*, *14*). Spiking correlations r_{in} between inputs, however, have a major impact on the output correlation r_{out} of the postsynaptic pair. When all inputs are E, weak input correlations give rise to strongly correlated synaptic currents and output spikes (Fig. 1C). This occurs because, when p and r_{in} are small, the correlation c of the two input currents is approximately equal to

$$c \simeq p + Nr_{in} \qquad (1)$$

(*15*), where N is the number of synaptic inputs, resulting in a large gain in the relation between r_{in} and r_{out} (Fig. 1E, upper solid curve). The situation changes when both neurons receive I as well as E inputs. Correlations between E or between I neurons lead to strongly cor-

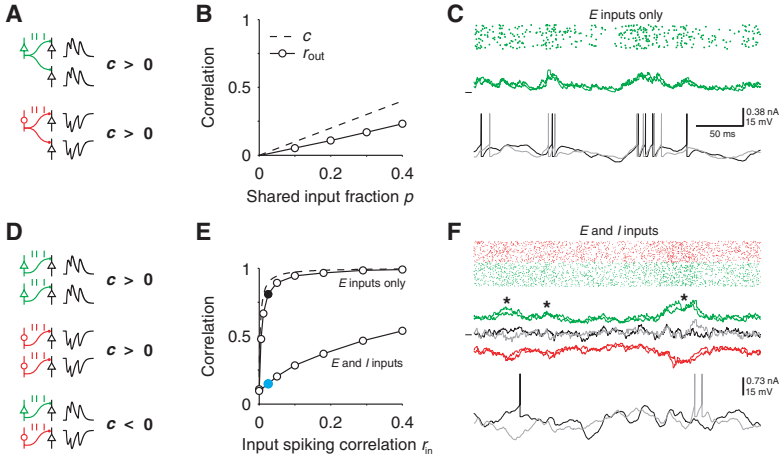

Fig. 1. Effect of shared inputs and correlated inputs on output correlation. (**A**) Shared excitatory (E, green) or inhibitory (I, red) inputs induce positive correlations in the synaptic currents of two cells ($c > 0$). (**B**) Correlation coefficient of synaptic currents c (dashed line) and output spikes r_{out} (circles, count window 50 ms) of a postsynaptic pair of integrate-and-fire neurons as a function of the shared input fraction p (*21*). Each postsynaptic cell received $N_E = 250$ Poisson input spike trains. (**C**) Input spike raster (top), synaptic currents (middle), and membrane potentials (bottom) of a postsynaptic pair receiving weakly correlated E inputs [black circle in (E), $r_{in} = 0.025$]. (**D**) Whereas correlations between E inputs or between I inputs contribute positively to c, correlations between E and I inputs have a decorrelating effect. (**E**) Correlations c (dashed line) and r_{out} (circles) as a function of the input spike correlation r_{in} at fixed $p = 0.2$. E inputs only: Each cell receives $N_E = 250$ correlated Poisson spike trains (*21*); E and I inputs: $N_I = 220$ inhibitory input trains were added with identical statistics and correlations. (**F**) Same as (C) but for the case with E and I inputs [blue circle in (E), $r_{in} = 0.025$]. E and I currents are shown separately from the total currents (black and gray). Asterisks indicate large fluctuations in the excitatory and inhibitory currents that occur simultaneously.

[1]Center for Molecular and Behavioral Neuroscience, Rutgers University, Newark, NJ 07102, USA. [2]Center for Neural Science, New York University, New York, NY 10003, USA. [3]Institute of Experimental Medicine, Hungarian Academy of Sciences, Budapest 1083, Hungary. [4]Departamento de Física Teórica, Universidad Autónoma de Madrid, Madrid 28049, Spain. [5]Smilow Research Center, New York University Medical School, New York, NY 10016, USA.

*These authors contributed equally to this work.
†Present address: Departments of Bioengineering and Electrical and Electronic Engineering, Imperial College, London SW7 2AZ, UK.
‡To whom correspondence should be addressed. E-mail: arenart@andromeda.rutgers.edu

related excitatory and inhibitory synaptic currents (Fig. 1F, red and green traces). However, when E and I inputs are themselves correlated, large fluctuations in the excitatory and inhibitory currents occur simultaneously (Fig. 1F, asterisks) and cancel, which leads to a significant reduction in the correlation of the total synaptic currents c and output spikes (Fig. 1F, black and gray traces). Correlations between E and I inputs thus decorrelate the synaptic currents to postsynaptic neurons (*16*).

To investigate whether such decorrelation can arise spontaneously from the dynamics of a recurrent network, we characterized the behavior of correlations in a simple recurrent circuit of binary neurons (*17*–*19*). The network consists of two populations (of size N) of E and I neurons connected randomly, both receiving excitatory projections from an external (X) population of N cells (Fig. 2A). The network has two key properties: First, the connectivity is "dense" so that the connection probability p (and thus the mean fraction of shared input) is fixed independently of the network size [e.g., $p = 0.2$ (*20*) as in Fig. 2]. Second, the synaptic couplings are "strong," such that only a small fraction of a cell's excitatory inputs is enough to evoke firing (Fig. 2B); in the model, although the average number of inputs is proportional to N, the number of E inputs needed to induce firing is only proportional to $\sqrt{N}$ (*19*). Our analysis showed that, even in the presence of shared input, the network settles into a stationary state in which the population-averaged firing correlation $\bar{r}$ is weak, if inhibition is sufficiently strong and fast. In fact, in networks of different sizes, $\bar{r}$ decreases in a way inversely proportional to N (Fig. 2C, open squares) [(*17*) section 2.3], a signature of asynchronous networks (*18*). In an asynchronous state, the variance of the population-averaged instantaneous activity scales in the same way as if the neurons were completely independent—as $1/N$. Thus, correlations in the asynchronous state do not qualitatively constrain averaging of activity across neural populations (fig. S2) (*18*).

Asynchronous activity persists in the presence of shared input because of a spontaneously generated tracking of fluctuations in the population-averaged instantaneous activities $m_E(t)$ and $m_I(t)$ of the E and I neurons (Fig. 2D) [(*17*) section 2.4]. Specifically, $m_I(t)$ tracks $m_E(t)$ with a small lag (*EI-Lag*), and they both closely follow the external instantaneous activity $m_X(t)$. In larger networks, tracking becomes more accurate and becomes perfect in the large N limit,

$$m_E(t) = A_E\, m_X(t);\; m_I(t) = A_I\, m_X(t) \qquad (2)$$

where A_E and A_I are constants that depend on the network architecture. Tracking occurs because, when the connectivity is strong and dense, even small "random" fluctuations in instantaneous excitatory activity, of order $1/\sqrt{N}$, are large enough to recruit inhibitory feedback.

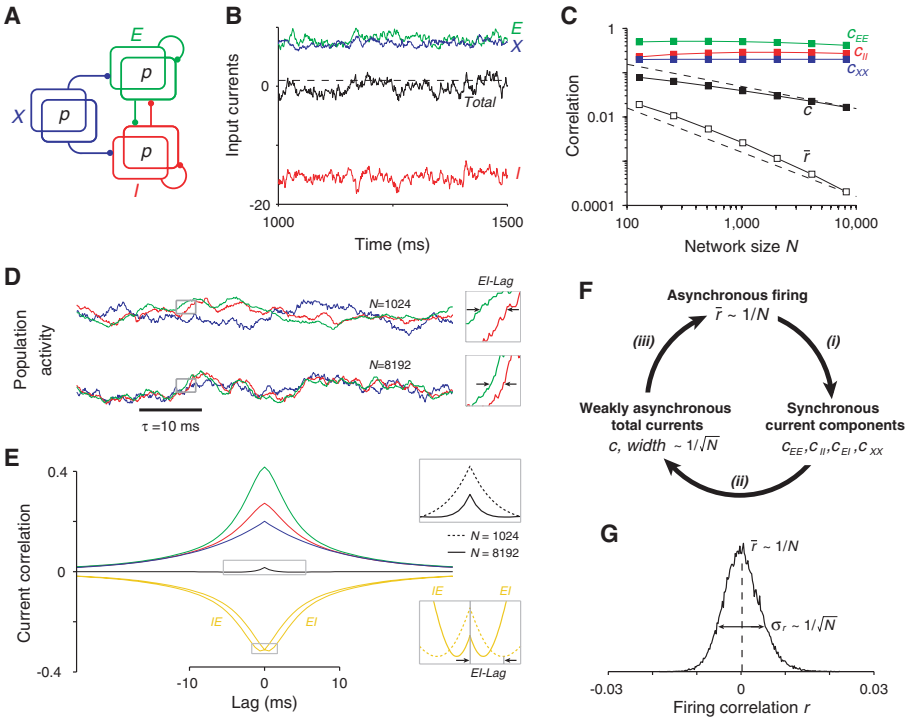

Fig. 2. Asynchronous activity in a binary recurrent network. (**A**) Schematic of the network architecture. The shared input fraction is p. (**B**) Strong coupling produces irregular spiking activity because of a dynamic balance between the large excitatory (*E* and *X*) and inhibitory (*I*) currents to each cell (*19*, *22*). Dashed line represents threshold. (**C**) Population-averaged correlation coefficients of the firing activity ($\bar{r}$, open squares); total current (*c*, filled squares); and current components versus network size *N*. Dashed lines show $1/\sqrt{N}$ and $1/N$ scaling for comparison. (**D**) Instantaneous population-averaged activities (transformed to *z* scores) of the *E*, *I*, and *X* neurons showing that tracking becomes more accurate with increasing *N*. (Insets) Instances of the lag between *E* and *I* activities (*EI-Lag*). Color code as in (B). (**E**) Population-averaged CCGs of the current components ($N = 8192$). Color code as in (C). (Insets) Magnification of the peak of the *IE* and *EI* CCGs (bottom) shows that the *EI-Lag* decreases with *N*, which leads to the decrease in the magnitude and width of the total current CCG (top). (**F**) Description of the asynchronous self-consistent solution (see text). (**G**) The histogram of firing correlations in the network (*EE* pairs; $N = 8192$) is wide: $\sigma_r >> \bar{r}$.

Tracking of the instantaneous population activities is equivalent to a precise cancellation of the different components of the (zero-lag) population-averaged current correlation c (Fig. 2E) [(*17*) section 2.5]. Because the synaptic current to each cell consists of an excitatory and an inhibitory component, the average current correlation across cell pairs, c, can be decomposed into c_{EE}, c_{II}, and c_{EI} (the term $c_{IE} = c_{EI}$). Both c_{EE} and c_{II} are positive and large, i.e., independent of N, for large networks (Fig. 2C, colored squares) because of amplification of weak firing correlations and of shared E or I inputs (Fig. 2F, *i*; and Fig. 1F, red and green traces). However, c_{EI} is large and negative because of correlations between E and I cells generated by tracking, which leads to the cancellation:

$$c = c_{EE} + c_{II} + 2c_{EI} \sim 1/\sqrt{N} \qquad (3)$$

(Fig. 2C, filled squares; 2F, *ii*; and fig. S3). Even after this cancellation, however, the instantaneous current correlation c is still larger than the correlation in firing $\bar{r}$ (Fig. 2C, filled and open squares). This is possible because neurons integrate their inputs over time, so that the instantaneous correlation $\bar{r}$ is related to the area under the current cross-correlogram (CCG). Because tracking becomes faster for larger networks, both the width of the current CCG (effectively set by the *EI-Lag*) and its magnitude decrease as $1/\sqrt{N}$ (Fig. 2E, insets). Its area is thus $1/N$, as required for asynchronous firing (Fig. 2F, *iii*). Because the asynchronous state just described is a dynamical phenomenon, it does not require fine-tuning of network parameters (fig. S4). Parameter changes lead to adjustments in rates and correlations such that the cancellation in Eq. 3 still holds.

Although the theory predicts that the population-averaged correlation $\bar{r}$ should be close to zero, it does not predict that every pair of cells should be as weakly correlated. Rather, the distribution of r across pairs is "wide," with a standard deviation σ_r much larger than its mean $\bar{r}$ for large networks (σ_r decays only as $1/\sqrt{N}$), which results in similar numbers of positively and negatively correlated pairs (Fig. 2G). This is because the hard-wired sources of correlation have a strong impact on individual r values (of order $1/\sqrt{N}$) and

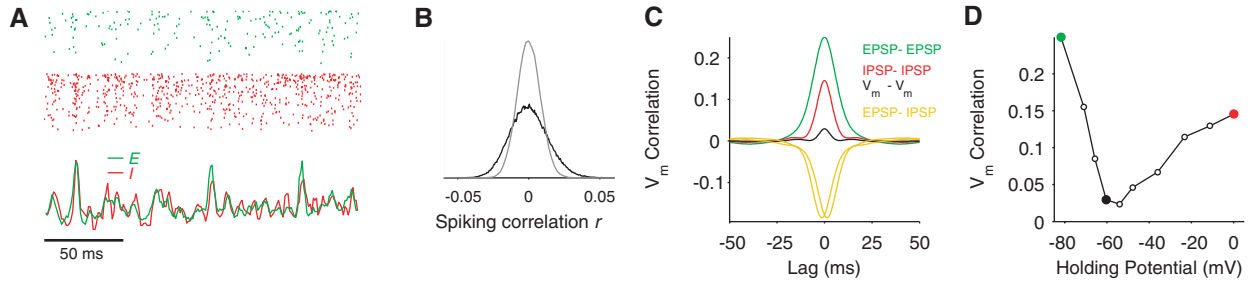

Fig. 3. Cancellation of correlations in a recurrent network of spiking neurons. (**A**) Raster (top) of 500 *E* (green) and *I* (red) neurons sorted by rate in a conductance-based integrate-and-fire network receiving shared independent Poisson inputs (p = 0.2). Bottom curves show tracking of instantaneous population-averaged activities (transformed to z scores, bin size 3 ms). Average firing rates of *E* and *I* cells were 1 and 3.6 spike per s, respectively. (**B**) Histogram of spike count correlations (black; count window 50 ms) and of jittered spike trains [gray, jitter ± 500 ms (*21*)]. (**C**) Population-averaged CCGs of the membrane potential containing mostly EPSPs (green) or IPSPs (red) in both cells, or EPSPs for one cell and IPSPs for the other (gold). The black curve is from pairs at resting potential. (**D**) Peak height of the membrane potential CCG as a function of the mean holding potential of both neurons in the pair. Green and red circles correspond to the reversal of inhibition and excitation, and the black circle corresponds to rest.

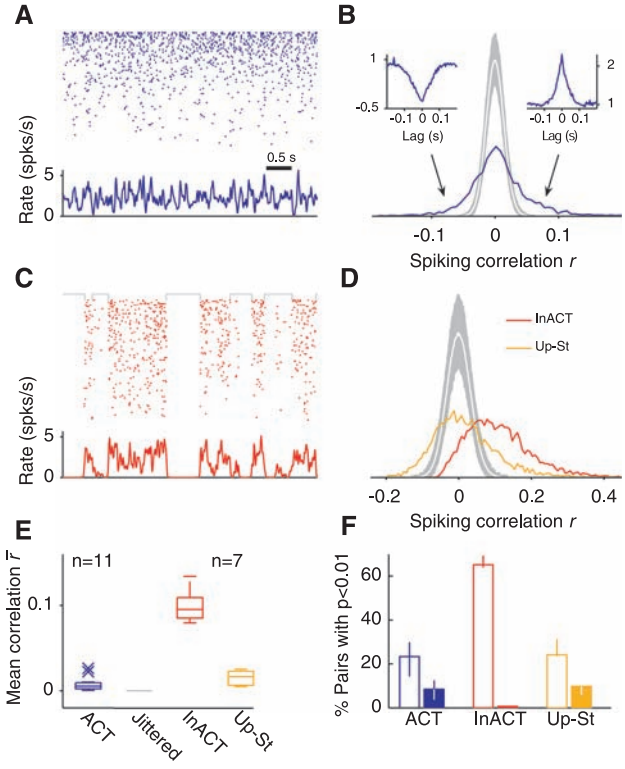

Fig. 4. Distribution of correlations in the rat neocortex in vivo. (**A**) Raster (top) and instantaneous population activity (bottom) for a population of 100 simultaneously recorded neurons (sorted by rate) during a period of cortical activation (ACT). (**B**) Histogram of spike count correlations of the population in (A) is wide ($\sigma_r >> \bar{r}$). The white curve is the mean histogram of the jittered spike trains [jitter ± 200 ms, gray shade 95% confidence interval; count window 50 ms (*21*)]. Insets show average raw cross-correlograms of all negatively (left) and positively (right) significantly correlated pairs (P < 0.01). (**C** and **D**) Same as (A and B) for the same population of cells during a period of cortical inactivation (InACT). Histogram of correlations during InACT is biased toward positive values (red). Restricting the analysis to up-state activity by removing down-state periods [black brackets in (C), (*21*)] largely eliminates the positive bias (Up-St, orange). (**E**) Box-whisker plots showing the distribution of mean correlations across experiments for different conditions. Crosses represent outliers. (**F**) Median fraction of significantly correlated pairs (P < 0.01, white bars) and of significantly and negatively correlated pairs (filled bars) across experiments. Error bars represent interquartile range.

therefore generate large heterogeneity across pairs (fig. S3). Asynchronous activity is also possible under nonstationary conditions: Numerical simulations with time-varying inputs display a similar correlation structure if r is computed with respect to the time-varying instantaneous average activity of each cell (fig. S5).

Active decorrelation of synaptic currents also occurs in a more biologically plausible network of spiking neurons. We simulated large networks of randomly connected conductance-based integrate-and-fire neurons (*21*), with parameters chosen to produce a balanced state (*19*, *22*) where neurons fired irregularly (Fig. 3A). As predicted, the distribution of spike count correlation coefficients r is wide (Fig. 3B), with an extremely low average (in *EE* pairs $\bar{r}$ < 0.001 for all count window sizes, fig. S6C). This happened for a large range of average firing rates and connection probabilities (fig. S7, A to F), with synchrony developing only when inhibition was substantially slower than excitation (fig. S7, G to I). The distribution of r conditioned on the response to time-varying external inputs was also wide for a large range of modulation frequencies (fig. S8). To determine whether a cancellation between the components of the current correlation (Eq. 3) underlies the small value of $\bar{r}$ observed, we injected different levels of constant current into cell pairs in which we had disabled the spiking mechanism. The range of current levels was adjusted to isolate the excitatory postsynaptic potential (EPSP) and the inhibitory postsynaptic potential (IPSP) components near their respective reversal potentials (*23*), or combinations of EPSPs and IPSPs at intermediate potentials. The correlation between isolated EPSPs (Fig. 3C, green) and between isolated IPSPs (red) was much larger than the correlation measured with no injected current (black), because of a cancellation with the large negative correlation between EPSPs and IPSPs (gold). The V-shaped relation between membrane potential correlation and holding potential (Fig. 3D) is an experimentally testable prediction of our theory.

The existence of a wide distribution of spike count correlations was confirmed in neuronal population recordings collected with silicon microelectrodes in somatosensory and auditory cortices of urethane-anesthetized rats (*21*). Under urethane anesthesia, cortical activity displays spontaneous changes in state (*24*) homologous to those seen during sleep (*25*). Network activity alternates between an "activated" (ACT) state of tonic firing, resembling that seen in rapid eye movement (REM) sleep (Fig. 4, A and B, blue), and an "inactivated" state (InACT), characterized by global fluctuations in population activity (up-down transitions) resembling slow-wave sleep (Fig. 4, C and D, red). During ACT periods, correlations were, on average, remarkably small, and the correlation histogram was wide. (Fig. 4B shows one experiment: $\bar{r}$ = 0.0075; 47% of pairs negatively correlated.) These values were typical of ACT state correlations across different animals [(Fig. 4E) n = 11 recording sessions in nine rats, $\bar{r}$ median was 0.0053 (0.0024 to 0.0094 interquartile range); across all 30,772 pairs, $\bar{r}$ = 0.0052, and 47% had r < 0]. This behavior did not depend strongly on the time scale at which correlations were measured (fig. S9). Although $\bar{r}$ in the ACT state was systematically low, it was positive and significantly different from zero

in all experiments (Fig. 4E; $P < 0.005$). A minority of both positive and negative correlations were statistically significant (Fig. 4, B and F, blue versus gray). Pairs with significant negative (positive) correlations showed clear troughs (peaks) in their cross-correlograms on average (Fig. 4B, insets, and fig. S10). Finally, the correlation histogram during the ACT state was still wide, even if only neurons recorded in the same shank were considered (fig. S11). During InACT periods, as expected from comodulation by the slow oscillation, the distribution of r was consistently biased toward positive values [(Fig. 4, C to F, red) for seven sessions in five rats, $\bar{r}$ median was 0.0953 (0.088 to 0.109 interquartile range); across all 18,916 pairs, $\bar{r} = 0.096$, and 9% had $r < 0$]. Within up-state periods, however, average correlations were again weak (*26*); removal of down-states from the recorded spike trains (*21*) resulted in correlation histograms similar to those during the ACT state [(Fig. 4, D and E, orange) $\bar{r}$ median was 0.0163 (0.0066 to 0.023 interquartile range); across all 18,916 pairs, $\bar{r} = 0.0136$, and 45% had $r < 0$]. Thus, correcting for common modulations in activity revealed a wide distribution of correlations even under nonstationary conditions in vivo.

In summary, we demonstrate theoretically that recurrent network dynamics can lead to an active decorrelation of synaptic currents, resulting in a state of arbitrarily low mean correlation. We therefore conclude that shared input does not inevitably cause correlated activity. By preventing uncontrolled network-wide synchrony, this mechanism generates a background of weakly correlated spiking, as required for efficient information processing based on either firing rates or coordinated spike timing patterns (*27*, *28*). Both simulations and in vivo recordings showed a wide distribution of correlations under stationary conditions. In nonstationary conditions, global activity modulations can result in positively biased correlations, but correlations around the mean activity imposed by these modulations can still be extremely small (Fig. 4, D and E; and figs. S5 and S8). Similarly weak correlations have been reported in visually driven neural populations in area V1 of awake behaving monkeys (*29*). However, as the constellation of inputs driving a cortical circuit is, in general, unknown to the experimenter, positive correlations may persist even after all experimentally controlled variables are accounted for (*11*, *12*). Whether "residual" correlations of this nature will have a strong impact on coding will depend on the extent to which downstream networks are able to disambiguate modulations in activity due to different sources. In either case, we suggest that cortical circuitry does not itself constitute an irreducible source of "noise."

References and Notes

1. T. J. Gawne, B. J. Richmond, *J. Neurosci.* **13**, 2758 (1993).
2. E. Zohary, M. N. Shadlen, W. T. Newsome, *Nature* **370**, 140 (1994).
3. E. Vaadia *et al.*, *Nature* **373**, 515 (1995).
4. D. Lee, N. L. Port, W. Kruse, A. P. Georgopoulos, *J. Neurosci.* **18**, 1161 (1998).
5. C. M. Gray, W. Singer, *Proc. Natl. Acad. Sci. U.S.A.* **86**, 1698 (1989).
6. A. Riehle, S. Grün, M. Diesmann, A. Aertsen, *Science* **278**, 1950 (1997).
7. K. H. Britten, M. N. Shadlen, W. T. Newsome, J. A. Movshon, *J. Neurosci.* **12**, 4745 (1992).
8. H. Sompolinsky, H. Yoon, K. Kang, M. Shamir, *Phys. Rev. E* **64**, 051904 (2001).
9. M. N. Shadlen, W. T. Newsome, *J. Neurosci.* **18**, 3870 (1998).
10. B. Kriener, T. Tetzlaff, A. Aertsen, M. Diesmann, S. Rotter, *Neural Comput.* **20**, 2185 (2008).
11. P. R. Roelfsema, V. A. F. Lamme, H. Spekreijse, *Nat. Neurosci.* **7**, 982 (2004).
12. M. R. Cohen, W. T. Newsome, *Neuron* **60**, 162 (2008).
13. H. Nienborg, B. G. Cumming, *Nature* **459**, 89 (2009).
14. R. Moreno-Bote, N. Parga, *Phys. Rev. Lett.* **96**, 028101 (2006).
15. The correlation between two quantities, each given by sum of N variables correlated by an amount r_{in}, out of which Np are common, is equal to $[p + r_{in}(N - p)]/[1 + r_{in}(N - 1)]$, which is approximately equal to $p + Nr_{in}$ when $p \sim r_{in}N << 1$.
16. When the firing statistics of the E and I populations are identical, the leading order effect of positive firing correlations on c can only be ≥ 0. If excitation and inhibition are precisely balanced, the equality is realized and the fraction of shared input sets the population-averaged firing correlation (*9*).
17. Details of the theory are available in the Supporting Online Material on *Science* Online.
18. I. Ginzburg I, H. Sompolinsky, *Phys. Rev. E* **50**, 3171 (1994).
19. C. van Vreeswijk, H. Sompolinsky, *Science* **274**, 1724 (1996).
20. C. Holmgren, T. Harkany, B. Svennenfors, Y. Zilberter, *J. Physiol.* **551**, 139 (2003).
21. Materials and methods are available as supporting material on *Science* Online.
22. D. J. Amit, N. Brunel, *Cereb. Cortex* **7**, 237 (1997).
23. M. Okun, I. Lampl, *Nat. Neurosci.* **11**, 535 (2008).
24. M. Steriade, *Electroencephalography* (Williams & Wilkins, Baltimore, MD, ed. 4, 1999).
25. E. A. Clement *et al.*, *PLoS ONE* **3**, e2004 (2008).
26. E. A. Stern, D. Jaeger, C. J. Wilson, *Nature* **394**, 475 (1998).
27. T. P. Vogels, L. F. Abbott, *J. Neurosci.* **25**, 10786 (2005).
28. A. Kumar, S. Rotter, A. Aertsen, *J. Neurosci.* **28**, 5268 (2008).
29. A. S. Ecker *et al.*, *Science* **327**, 584 (2009).

30. We thank A. Amarasingham, N. Brunel, G. Buzsaki, B. Doiron, A. Ecker, S. Fijisawa, A. Heimel, A. Kohn, D. Robbe, S. Sakata, E. Stark, and A. Tolias for comments on an earlier version of this manuscript; C. van Vreeswijk for discussions; and A. Compte, S. Ardid, and J. Manrique for sharing their codes. This study was supported by NIH grants MH073245 and DC009947; NSF grant SBE-0542013 to the Temporal Dynamics of Learning Center, an NSF Science of Learning Center; a National Institute on Deafness and Other Communication Disorders, NIH, grant DC-005787-01A1; and a Spanish grant FIS 2006-09294. K.D.H. is an Alfred P. Sloan fellow. We would like to dedicate this work to the memory of D. J. Amit.

Supporting Online Material

www.sciencemag.org/cgi/content/full/327/5965/587/DC1
Materials and Methods
SOM Text
Figs. S1 to S11
References

29 July 2009; accepted 10 December 2009
10.1126/science.1179850

Direct Restart of a Replication Fork Stalled by a Head-On RNA Polymerase

Richard T. Pomerantz and Mike O'Donnell*

In vivo studies suggest that replication forks are arrested by encounters with head-on transcription complexes. Yet, the fate of the replisome and RNA polymerase (RNAP) after a head-on collision is unknown. We found that the *Escherichia coli* replisome stalls upon collision with a head-on transcription complex, but instead of collapsing, the replication fork remains highly stable and eventually resumes elongation after displacing the RNAP from DNA. We also found that the transcription-repair coupling factor Mfd promotes direct restart of the fork after the collision by facilitating displacement of the RNAP. These findings demonstrate the intrinsic stability of the replication apparatus and a previously unknown role for the transcription-coupled repair pathway in promoting replication past a RNAP block.

In vivo studies suggest that replication forks are arrested by head-on transcription complexes, but are unaffected by codirectional transcription complexes (*1*) [supporting online material (SOM) Text S1]. Mechanisms that resolve head-on collisions in favor of the replisome are therefore necessary for chromosome duplication and may preserve genomic integrity by preventing fork collapse. In vivo data indicate that head-on replisome–RNA polymerase (RNAP) collisions cause chromosomal deletions, which suggests dissociation of the replisome (*2*). Genetic studies implicate recombinational repair in resolving conflicts between replication and transcription, which also suggests the possibility of fork collapse (*3*, *4*). Similarly, in vitro data imply that the replisome dissociates after encountering a *lac* repressor, which arrests the fork (*5*). In contrast, several in vivo studies indicate that although replication forks stall at protein barriers, the replisome remains stable and resumes elongation after removal of the block (*6*). Thus, replisome stalling may not necessitate fork collapse (*7*). We investigated the stability of the *Escherichia coli* replisome after it encounters a head-on RNAP in vitro.

The Rockefeller University, Howard Hughes Medical Institute, 1230 York Avenue, New York, NY 10021 USA.

*To whom correspondence should be addressed. E-mail: odonnell@mail.rockefeller.edu